

Superradiant scattering of orbital angular momentum beams

Cisco Gooding,^{1,2} Silke Weinfurtner,^{1,3} and William G. Unruh²

¹*School of Mathematical Sciences, University of Nottingham, UK*

²*Department of Physics & Astronomy, University of British Columbia, Canada*

³*Centre for the Mathematics and Theoretical Physics of Quantum Non-Equilibrium Systems, University of Nottingham, UK*

(Dated: December 15, 2024)

We discuss the wave-structure coupling between an orbital angular momentum beam and a rapidly rotating disk. Motivated by exploring unknown features of how angular momenta affect wave-structure interactions, we present a new configuration exhibiting the wave amplification effect known as rotational superradiance. While rotational superradiance was initially envisioned in terms of the scattering of an incident wave directed perpendicular to an object's rotation axis, we demonstrate in the context of acousto-mechanics that the same effect occurs for a vortex beam directed parallel to the rotation axis. We propose two different experimental routes: one must either work with rotations high enough that the tangential velocity at the outer edge of the disk exceeds the speed of sound, or use evanescent sound waves. We then argue that the latter possibility is more promising, and provides the opportunity to probe a previously unexamined parameter regime in the acoustics of rotating porous media. An experimental implementation thereof will answer some of the open questions related to interactions of rapidly rotating wave-structure interactions.

Introduction.—An orbital angular momentum (OAM) beam is a traveling wave with angular momentum in the direction of its propagation. Rather than angular momentum associated with spin degrees of freedom, OAM beams result from spatial wave distributions that have a helical structure. OAM beams can be formed in nearly any effective field theory with propagating modes, such as electromagnetism (i.e. light beams) and fluid dynamics (i.e. sound beams in air or water), and as such have facilitated the widespread application of rotation for science and industry alike. Despite their interest and applicability there is still much to be learned about how OAM beams interact with rapidly rotating objects. In this letter, we present a novel approach demonstrating the amplification or overreflection of OAM beams from a rapidly rotating disk.

Our proposal complements the well-known configuration used to describe rotational superradiance, a celebrated theoretical effect that can occur in gravitational [1, 2], electromagnetic [3, 4], and fluid dynamical systems [5]. Theoretical work on rotational superradiance began in the 1970s, though the effect has eluded experimental confirmation until only recently. The first detection of rotational superradiance was achieved for surface waves interacting with a vortex flow [6]. One of the major difficulties inherent to superradiance experiments stems from geometry: given a rotating, partially absorbing object, the standard approach follows Zel'Dovich's original conception, which involves scattering a wave directed perpendicular to the object's rotation axis. Consequently, the incident wave scatters in a continuum of directions, making detection and subsequent analysis of the scattered wave problematic.

Instead of perpendicular, we propose to direct an incident wave (carrying angular momentum) parallel to the

object's rotation axis. Hence, within this configuration it is possible to utilise the arguably advantageous OAM beams to probe for superradiance. In cylindrical coordinates (r, θ, z) with the z -axis aligned with the object's angular momentum, our new configuration amounts to scattering in the z -direction, as opposed to in the (r, θ) plane. We therefore reduce the *effective* dimensionality of the scattering setup, resulting in a conceptual as well as *practical* simplification that admits a more transparent theoretical description. The simplifications our approach brings with it broaden the range of possible applications.

Below we will apply our new framework for superradiance to the fluid dynamical model of acoustic vortex beams to demonstrate the simplicity of the theoretical description that follows from aligning the directions of the incident and scattered waves, and make comparisons with previous fluid dynamical approaches. We prove that in the superradiant regime, one cannot both operate the disk with solely subsonic tangential velocities and use propagating modes for the wave scattering. One must therefore either rotate the disk fast enough for part of it to travel supersonically, or else work with evanescent waves. We then focus on the experimental implementation of our proposal for sound waves in air. We provide a new expression for the surface impedance at the air-disk interface, and calculate the amplification spectra for experimentally feasible parameters. This is followed by a detailed discussion of vortex beam generation and detection of the scattered wave. By taking all of the above into account we argue that the implementation of our proposal is within experimental reach. Finally, we comment on the applicability of our proposal to electromagnetic systems, which could potentially allow quantum aspects of superradiance to be observed.

Theoretical model.—The fluid we consider to be barotropic, and bounded by a cylindrical tube of inner

radius R . At one end of the tube a coaxial rotating disk composed of sound-absorbing material is inserted. The disk is aligned with a cylindrical coordinate system (r, θ, z) such that the surface of the disk is located at $z = 0$. At the opposite end of the tube (which is pointing at the positive z -direction) acoustic waves are produced, and are guided through the cylinder towards the fluid-disk interface. Away from the disk we assume a uniform background density ρ_0 and vanishing background flow \mathbf{u}_0 . The acoustic velocity \mathbf{u} is then irrotational, and can be expressed in terms of a potential Φ as $\mathbf{u} = \nabla\Phi$.

For a monochromatic sound wave with frequency ω and total wavenumber k , we can write the acoustic pressure as $p = c^2\rho = i\omega\rho_0\Phi$, with $c = \omega/k = \sqrt{B_a/\rho_0}$ the phase speed and B_a the (adiabatic) bulk modulus of the fluid. The velocity potential for such a monochromatic sound wave obeys the Helmholtz equation $\nabla^2\Phi + k^2\Phi = 0$.

The fluid is enclosed by the tube at $r = R$, so we enforce the impermeability boundary condition,

$$\mathbf{u} \cdot \hat{\mathbf{r}}|_{r=R} = \partial_r\Phi|_{r=R} = 0. \quad (1)$$

At the surface of the disk, determination of the boundary condition is less straightforward. To absorb sound, we assume a disk made of a porous/fibrous material. There is a large amount of literature devoted to the dynamics of fluids in saturated porous materials (see [7] and references therein), though motion of the porous frame is neglected in most work. A notable exception is Auriault's analysis of acoustic waves in the saturating fluid coupled with elastic waves in deformable, poroelastic media undergoing steady rotation at an angular velocity $\boldsymbol{\Omega}$ [8]. Auriault uses a technique known as homogenization, which involves averaging over a representative volume element (RVE) containing sufficient pores to allow for a coarse-grained description at the macroscopic scale [9]. We follow Auriault's approach to characterize the fluid-structure interaction at the disk surface, but since we ultimately wish to implement our proposal with sound waves in air, the frame can be treated as rigid: the bulk moduli of most porous materials are much larger than the bulk modulus of air, so elastic waves in the frame are not excited by acoustic waves in the fluid [10].

One then expects a macroscopic description of the acoustics in terms of an effective fluid propagating on a rotating background. Defining features of the effective fluid are determined by the extent of drag and other interactions with the rotating porous frame. Within non-rotating anisotropic rigid-framed porous media, quasi-stationary fluid motion obeys Darcy's law,

$$\mathbf{v} = -\frac{1}{\mu} \mathbf{K}(\omega) \cdot \nabla p, \quad (2)$$

where μ is the fluid viscosity, $\mathbf{K}(\omega)$ is the permeability tensor, and the filtration velocity \mathbf{v} (also known as the Darcy velocity) represents the pore-scale fluid velocity averaged over a RVE [11, 12]. Isotropy at the macro-

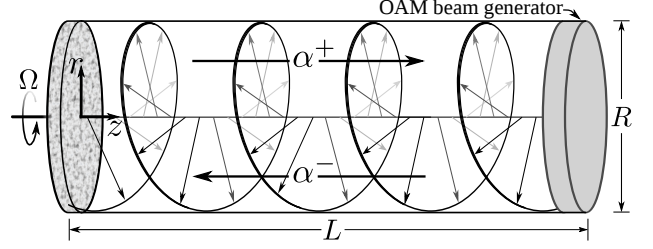


FIG. 1. Schematic representation of the scattering setup.

scopic level corresponds to a scalar permeability, multiplied by the unit tensor. We describe in the Supplemental Material how linearity between the pressure gradient and the filtration velocity is still maintained when the disk undergoes a rigid rotation with constant angular velocity $\boldsymbol{\Omega}$. The tensor defining the linearity between ∇p and \mathbf{v} can still be interpreted as a (dynamic) permeability \mathbf{K} , but unlike the non-rotating case, \mathbf{K} is not symmetric, and depends on $\boldsymbol{\Omega}$.

We enforce continuity of mass flux at the air-disk interface. This is equivalent to continuity of normal fluid velocity, for acoustic oscillations that are harmonic. In [5], sound absorption by a rotating porous object is described in the co-rotating frame by an impedance condition $p = -\bar{Z}\mathbf{u} \cdot \mathbf{n}$, where \mathbf{n} is the unit surface normal and the co-rotating surface impedance \bar{Z} is a frequency-dependent complex function that encapsulates how the surface interacts with impinging sound waves [13, 14]. For the monochromatic modes under consideration, the co-rotating impedance condition is

$$\left. \frac{\partial_z\Phi}{\Phi} \right|_{z=0} = \frac{-i\rho_0\bar{\omega}}{\bar{Z}}, \quad (3)$$

which rests on the assumption that an impedance condition applies in a frame co-rotating with the disk. In the Supplemental Material, we relax this assumption, and by careful analysis of fluid behaviour at the surface of the disk derive a laboratory-frame surface impedance given by

$$Z = \frac{\rho_0\bar{\omega}}{\varphi k_z} \left(1 + \frac{i\bar{\omega}_c}{\bar{\omega}} \right), \quad (4)$$

where $\bar{\omega} = \omega - m\Omega$ and \bar{k}_z are the co-rotating wave frequency and axial wavenumber, φ is the porosity (fraction of air volume to total volume in the disk), $\bar{\omega}_c = \mu\varphi/\rho_0 K_0$ is a characteristic frequency scale defined by the viscosity and the pore geometry, and K_0 is the (static) permeability of the disk.

For simplicity of presentation, we will work with the condition (3); deviations occurring due to the more accurate condition (4) are of interest in their own right, and can be explored when implementing our approach experimentally.

Superradiant amplification.— The Helmholtz equation for the acoustic potential has separable solu-

tions of the form $\Phi = J_m(k_r r) e^{im\theta} e^{ik_z z} e^{-i\omega t}$, where $J_m(k_r r)$ is a Bessel function of the first kind, and m is an integer that indicates the topological charge of the mode. The radial and axial wavenumbers are given by k_r and k_z , and are related to the total wavenumber k by the relation $k^2 = k_r^2 + k_z^2$. The boundary condition (1) then implies $J'_m(k_r R) = 0$. Denoting the n^{th} zero of J'_m by x_{mn} , we can equivalently express this condition as $k_r R = x_{mn}$, which makes explicit the constraint imposed on the allowed radial wavenumbers. Therefore, there are two kinds of modes in this setup: propagating modes, where $k_z = \sqrt{k^2 - k_r^2}$ is real, and evanescent modes, with purely imaginary k_z . In our setup the incoming wave travels in the negative z direction, and a reflected wave travels back in the positive z direction. The acoustic velocity potential can then be written as

$$\Phi = J_m(k_r r) e^{im\theta} e^{-i\omega t} (\alpha^- e^{-ik_z z} + \alpha^+ e^{ik_z z}). \quad (5)$$

The amplification factor is defined as $A_{\omega m} = \frac{|\alpha^+|^2}{|\alpha^-|^2} - 1$, and in our case it is given by

$$A_{\omega m} = \frac{-4\rho_0\bar{\omega}\text{Re}[k_z\bar{Z}]}{|\rho_0\bar{\omega} + k_z\bar{Z}|^2} = \frac{-4\text{Re}[\bar{\chi}]}{|1 + \bar{\chi}|^2}, \quad (6)$$

with $\bar{\chi} = \rho_0\bar{\omega}/k_z\bar{Z}$. Superradiance occurs if the amplification is positive ($A_{\omega m} > 0$). Since the real part of the impedance is positive for absorptive materials, expression (6) indicates that for propagating modes the amplification is positive whenever $\omega - m\Omega$ is negative. If the mode is evanescent, the amplification defined by (6) is positive whenever both $\omega - m\Omega$ and the imaginary part of the impedance are negative.

To plot amplification spectra arising within our setup, we define the following dimensionless quantities: $\hat{Z} = \bar{Z}/\rho_0 c$, $\sigma = \omega/m\Omega$, and $\sigma_* = cx_{mn}/m\Omega R$. It follows that

$$\bar{\chi} = \frac{(\sigma - 1)}{\hat{Z}\sqrt{\sigma^2 - \sigma_*^2}}. \quad (7)$$

For co-rotating ($m > 0$) modes, the parameter σ_* is positive, and provides a measure of the sound speed relative to the tangential velocity at the outer edge of the disk. The value $\sigma_* = 0$ represents the limit of large disk radius, whereby the axial wavevector k_z is much greater than the radial wavevector k_r . The dimensionless impedance of “typical” porous/fibrous materials is often taken to be $\hat{Z} = 1 - i$ [5]. As can be deduced from the Supplemental Material, the accuracy of this estimate depends on the frequency of the acoustic mode.

Amplification spectra for propagating modes in our setup. Figure 2 shows the amplification varying with σ for the typical impedance for various values of the dimensionless parameter σ_* . When $0 \leq \sigma_* \leq 1$, a cusp forms along the horizontal axis at $\sigma = \sigma_*$, in which case the axial wavevector vanishes ($k_z = 0$) and all of the mode energy comes from angular momentum ($k = k_r$). One can

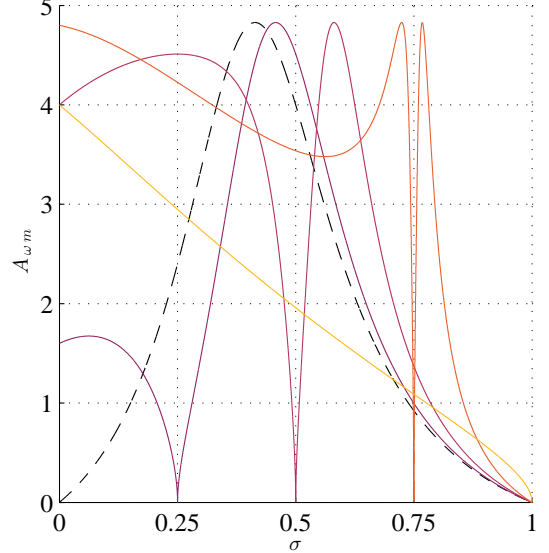


FIG. 2. Plot of the amplification factor for acoustic vortex beam superradiance using propagating modes, with $\hat{Z} = 1 - i$, and different choices of σ_* in the interval $[0, 1]$. For $0 < \sigma_* < 1$, the value of σ_* coincides with a cusp along the σ axis.

also observe from Figure 2 that maxima of the amplification factor have the same height for $0 \leq \sigma_* \leq 1$. The maximal amplification for this entire parameter range can then be determined by considering the $\sigma_* = 0$ case (the $R \rightarrow \infty$ limit), from which one easily obtains a maximal amplification of $A_{\omega m} = \sqrt{2}(2 + \sqrt{2})$. Upon comparison with the original superradiance setup [5], we find that the new scattering configuration can produce a nontrivial increase in the amount of superradiant amplification. For positive values of σ_* that are sufficiently less than unity, we also find a much broader maximum than in the original approach. A discussion of the amplification of the evanescent modes will be given in the following section.

Experimental implementation.—We will now discuss a specific experimental proposal for observing superradiance with OAM beams focussing on its feasibility using current technology. The geometrical arrangement of the experimental components is apparent from the schematics in Figure 1: OAM beam source, an effectively lossless cylindrical enclosure of given inner radius R length L , and a sufficiently rapidly rotating disk composed of sound absorbing material.

Techniques to produce OAM beams. Depending on the context, these types of waves are often referred to as either vortex beams, or in the specific case of acoustics, as “sonic screwdrivers”, due to the torque they can exert on sound absorbing objects [15]. OAM beam generation can be accomplished in two different ways. A *passive* technique, using either a spiral grating [16, 17], acoustic resonance [18], or a metamaterial [19]. The passive tech-

niques are relatively easy to construct and require less computational power, but this often comes at the cost of tunability, which would restrict exploration of the parameter space. This in contrast to the *active* technique, using a phase-controlled array of piezoelectric transducers [15, 20, 21]. If one seeks to test the accuracy of the impedance condition for a wide range of beam frequencies and rotation rates, a transducer array is the ideal method of beam generation.

Cylindrical enclosure. The cylindrical tubing serves to isolate the OAM modes from environmental noise sources, as well as providing infrastructure to monitor the acoustic pressure field. The measurement of the amplification factor can be achieved by attaching an array of microphones reaching the inner surface of the tube, which allows the pressure field to be reconstructed. The amplification factor can then be deduced by fitting the acoustic velocity potential Φ obtained from the acoustic pressure measurements via $\Phi = p/i\omega\rho_0$ with the predicted form (5). The phase speed c of acoustic waves in air is 343 m/s, and hence a characteristic length scale for both propagating and evanescent modes is given by c/f , where f is its frequency. Therefore, for our system to contain a manageable number of characteristics lengths, it is desirable to work in the kHz frequency range, which corresponds to a length scale of $\lesssim 1$ m. The radial confinement of the tube is limited by the fact that one end of the tube is closed by a rapidly rotating disk of the same radius.

Rotating disk specification. Beam frequencies any higher than the kHz range are undesirable, since the superradiance condition implies that we must rotate our porous/fibrous disk at approximately the same frequency, and higher rotation rates are difficult to stabilize. Due to drag, rapid rotations can also create centrifugal pumping, but this effect can be minimized by using a frame with cylindrical pores aligned with the rotation axis of the disk. Working with rotation rates near the kHz range requires an extremely strong material, since at the outer disk edge the centripetal acceleration ($a_c = R\Omega^2$) will be approaching $10^5 g$ (with $g = 9.8 \text{ m s}^{-2}$ being the acceleration due to gravity). Typical porous/fibrous materials cannot sustain the associated tensile loads, but a foam made from the less familiar silicon carbide appears to be able to accommodate our demands [22–24]. If \bar{a}_c is the maximum centripetal acceleration a specific disk can support, then for subsonic disk motion we must keep the rotation rate Ω below \bar{a}_c/c .

Though larger amplification is possible with propagating modes, we consider it preferable experimentally to work with the evanescent modes, for the following reason. Using the relation $k = \omega/c$ and the radial constraint $k_r R = x_{mn}$ we can write the axial wavevector as $k_z = (1/c)\sqrt{\omega^2 - (cx_{mn}/R)^2}$, which is real whenever $\omega > cx_{mn}/R$. In the superradiant regime $\omega - m\Omega < 0$, we then find that $R\Omega > c(x_{mn}/m)$ for propagating modes.

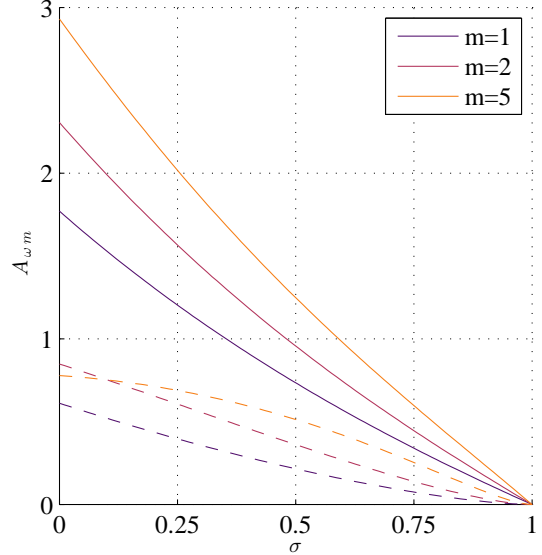


FIG. 3. Plot of the amplification factor for evanescent modes, including frequency variation in the surface impedance. Parameters: $\sigma_0 = 40 \text{ g/cm}^3$, $R = 8 \text{ cm}$, $\rho = 0.00129 \text{ g/cm}^3$, $c = 34300 \text{ cm/s}$, $\Omega/2\pi = 675 \text{ Hz}$, and $m = 1$ (red), $m = 2$ (black), $m = 5$ (blue). The solid lines use the dimensionless impedance $Z = 1 - i$. The dashed lines use empirical impedance functions [14], and are valid for $\sigma < 0.41$ ($m = 1$), $\sigma < 0.70$ ($m = 2$), and $\sigma < 0.88$ ($m = 5$).

The zeros of J'_m obey $x_{mn}/m > 1$, so we conclude that the tangential velocity $R\Omega$ at the outer edge of the disk must exceed the speed of sound c . Thus, part of the disk must move supersonically in order to superradiate propagating modes, which in general leads to instabilities [5]. It may be possible to eliminate the influence of instabilities by placing a membrane above the disk surface that transmits acoustic modes but prevents passage of fluid flow, but for experimental implementation these complications can be avoided by working solely with evanescent modes.

Measuring superradiance in the evanescent case requires a different approach than in the propagating case: if $k_z = i\kappa$, then the squared-norm of (5) is proportional to $\cosh 2\kappa(z - z_0) + \cos 2\alpha$, with $\alpha^+/\alpha^- = e^{2\kappa z_0 + 2i\alpha}$ (α is a phase-shift, and z_0 determines the amplification). By relating the acoustic potential Φ to the acoustic pressure p , one can locate the minimum z_0 in the pressure field within the tube to obtain the amplification.

In practice, the impedance of a sound-absorbing material varies with the frequency of the incident wave. To test whether such frequency dependence affects the preceding results, we consider the empirical impedance function for the porous/fibrous absorbent materials studied in [14], which has the complex power-law form $\hat{Z} \approx 1 + 9.08(f/\sigma_0)^{-0.75} - 11.9i(f/\sigma_0)^{-0.73}$. This empirical impedance is a function of the frequency

$f = \omega/2\pi$ scaled by the flow resistance σ_0 , and is valid for f in the range 250 – 4000 Hz, for materials with flow resistances of $2 - 80 \text{ g s}^{-1} \text{ cm}^{-3}$ (i.e. $2000 - 80,000 \text{ Pa s m}^{-2}$) [14]. We plot the resulting superradiant spectra for evanescent modes in Figure 3. While superradiance is slightly suppressed compared to the idealized case $\hat{Z} = 1 - i$, Figure 3 demonstrates that the amplification factor in our proposal can be larger than in the original configuration [5], for either propagating or evanescent modes.

Conclusion.— We have seen in the example of acousto-mechanics that our new direction for rotational superradiance leads to a simplified theoretical description. The associated effective dimensional reduction of the scattering arrangement also lowers the complexity of the experimental setup. We also derived a more accurate expression for the surface impedance at the air-disk interface at rapid relative rotation.

The results presented above indicate that our proposal offers a promising new way to explore superradiance experimentally. By following our suggested alignment of the wave propagation direction and disk rotation axis the amplification process is more efficient, leading to higher amplification compared to the standard approach. Guided by the theoretical model detailed in the Supplemental Material, our proposal also offers a new way to explore uncharted parameter regimes in the acoustics of rapidly-rotating porous media, which would further our understanding of the role angular momenta play in wave-structure interactions. Based on the similarities between acousto-mechanics and optomechanics [25], and the recent success measuring entanglement between rotating mirrors and laser modes with very high OAM [26–28], our new scattering direction may also allow quantum features of rotational superradiance to be observed in a laboratory setting.

ACKNOWLEDGEMENTS

The research of WGU is supported by NSERC (Natural Science and Engineering Research Council) of Canada, and also by CIFAR. SW acknowledges financial support provided under the Paper Enhancement Grant at the University of Nottingham, the Royal Society University Research Fellow (UF120112), the Nottingham Advanced Research Fellow (A2RHS2), the Royal Society Project (RG130377) grants, the Royal Society Enhancement Grant (RGF/EA/180286) and the EPSRC Project Grant (EP/P00637X/1). SW acknowledges partial support from STFC consolidated grant No. ST/P000703/. The fellowship held by CG while this research was conducted was funded by NSERC through WGU, with partial support from SW.

- [1] R. Penrose and R. M. Floyd, “Extraction of rotational energy from a black hole,” *Nature* **229**, 177 (1971).
- [2] J. Bekenstein, “Extraction of energy and charge from a black hole,” *Phys. Rev. D* **7**, 949 (1973).
- [3] Y. B. Zel'Dovich, “Generation of Waves by a Rotating Body,” *Zh. Eksp. Teor. Fiz.* **14**, 270 (1971) [JETP Lett. **14**, 180 (1971)].
- [4] Y. B. Zel'Dovich, “Amplification of Cylindrical Electromagnetic Waves Reflected from a Rotating Body,” *Zh. Eksp. Teor. Fiz.* **62**, 2076 (1972) [Sov. Phys. JETP **35**, 1085 (1972)].
- [5] V. Cardoso, A. Coutant, M. Richartz, and S. Weinfurter, “Detecting Rotational Superradiance in Fluid Laboratories,” *Phys. Rev. Lett.* **117**, 271101 (2016).
- [6] T. Torres, S. Patrick, A. Coutant, M. Richartz, E. W. Tedford, and S. Weinfurter, “Rotational superradiant scattering in a vortex flow,” *Nature Physics* **13**, 833 (2017).
- [7] D. A. Nield and A. Bejan, “Convection in Porous Media,” 4th Edition, Springer Science + Business Media, New York (2013).
- [8] J. -L. Auriault, “Acoustics of Rotating Deformable Saturated Porous Media,” *Transp. Porous Media* **61**, 235 (2005).
- [9] J. -L. Auriault, C. Boutin, and C. Geindreau, “Homogenization of Coupled Phenomena in Heterogenous Media,” Wiley and Sons, New Jersey, USA (2009).
- [10] J. F. Allard and N. Atalla, “Propagation of Sound in Porous Media: Modelling Sound Absorbing Materials,” Wiley-Blackwell, UK, 2nd ed. (2009).
- [11] H. Darcy, “Les Fontaines Publiques de la Ville de Dijon,” Dalmont, Paris (1856).
- [12] J. Bear, “Dynamics of Fluids in Porous Media,” Dover, New York (1972).
- [13] S. W. Rienstra and A. Hirschberg, “An Introduction to Acoustics,” (2018), <http://www.win.tue.nl/~sjoerdr/papers/boek.pdf>.
- [14] M. E. Delany and E. N. Bazley, “Acoustical properties of fibrous absorbent materials,” *Applied Acoustic* **3**, 105 (1970).
- [15] S. Gspan, A. Meyer, S. Bernet, and M. Ritsch-Marte, “An acoustical helicoidal wave transducer with applications for the alignment of ultrasonic and underwater systems,” *J. Acoust. Soc. Am.* **115**, 1142 (2004).
- [16] N. Jimenez, V. J. Sanchez-Morcillo, R. Pico, L. M. Garcia-Raffi, V. Romero-Garcia, and K. Staliunas, “High-order Acoustic Bessel Beam Generation by Spiral Gratings,” *Phys. Proc.* **70**, 245 (2015).
- [17] X. Jiang, J. Zhao, S. -l. Liu, B. Liang, X. -y. Zou, J. Yang, C. -W. Qiu, and J. -c. Cheng, “Broadband and stable acoustic vortex emitter with multi-arm coiling slits,” *Appl. Phys. Lett.* **108**, 203501 (2016).
- [18] X. Jiang, Y. Li, B. Liang, J. C. Cheng, and L. Zhang, “Convert Acoustic Resonances to Orbital Angular Momentum,” *Phys. Rev. Lett.* **117**, 034301 (2016).
- [19] L. Ye, C. Qiu, J. Lu, K. Tang, H. Jia, M. Ke, S. Peng, and Z. Liu, “Making sound vortices by metasurfaces,” *AIP Advances* **6**, 085007 (2016).
- [20] C. E. M. Demore, Z. Yang, A. Volovick, S. Cochran, M. P. MacDonald, and G. C. Spalding, “Mechanical Evidence of the Orbital Angular Momentum to Energy Ratio

of Vortex Beams,” Phys. Rev. Lett. **108**, 194301 (2012).

[21] J. F. Pazos-Ospina, J. L. Ealo, and E. E. Franco, “Characterization of phased array-steered acoustic vortex beams,” J. Acoust. Soc. Am. **142**, 61 (2017).

[22] Ed. P. Stevenson, “Foam Engineering - Fundamentals and Applications,” Wiley and Sons, Southern Gate, UK (2012).

[23] Eds. M. Bruneau and C. Potel, “Materials and Acoustics Handbook,” Wiley and Sons, New Jersey, USA (2009).

[24] Eds. F. Schüth, K. S. W. Sing, and J. Weitkamp, “Handbook of Porous Solids,” Wiley-VCH, Weinheim (2002).

[25] L. Zhang and P. L. Marston, “Angular momentum flux of nonparaxial acoustic vortex beams and torques on axi-symmetric objects,” Phys. Rev. E **84**, 065601(R) (2011).

[26] M. Bhattacharya, P. L. Giscard, and P. Meystre, “Entangling the rovibrational modes of a macroscopic mirror using radiation pressure,” Phys. Rev. A **77**, 030303 (2008).

[27] M. Bhattacharya, P. -L. Giscard, and P. Meystre, “Entanglement of a Laguerre-Gaussian cavity mode with a rotating mirror,” Phys. Rev. A **77**, 013827 (2008).

[28] R. Fickler, G. Campbell, B. Buchler, P. K. Lam, and A. Zeilinger, “Quantum entanglement of angular momentum states with quantum numbers up to 10010,” Proc. Natl. Acad. Sci. U.S.A. **113**(48), 13642 (2016).

Supplemental Material

Acoustics of the Saturating Fluid in Rotating, Rigid-framed Porous Media

To determine the correct surface condition at the air-disk interface, we take the rigid-frame limit of Auriault’s equations (101)-(104) [8], which corresponds to setting the displacement of the solid frame to zero, with respect to the steady rotation at angular velocity Ω . One then finds the independent equations

$$\nabla \cdot (-i\bar{\omega}\varphi \mathbf{U}_f) = \frac{i\bar{\omega}\varphi\beta p}{\rho_0 c^2} \quad (S1)$$

and

$$-i\bar{\omega}\varphi \mathbf{U}_f = -\frac{1}{\mu} \mathbf{K}(\bar{\omega}, \Omega) \nabla p, \quad (S2)$$

where \mathbf{U}_f is the acoustic fluid displacement, φ is the porosity, μ is the dynamic viscosity of the fluid, and β is the dimensionless fluid compressibility. The permeability tensor \mathbf{K} depends on the co-rotating acoustic frequency $\bar{\omega} = \omega - m\Omega$, as well as the angular velocity vector Ω , though the explicit functional form given by Auriault applies only to an idealized and very particular situation. We now provide a more general expression for the permeability, resulting in a model capable of describing the scattering of acoustic vortex beams described in our experimental proposal.

At the pore scale, the local dynamics for acoustic disturbances in a viscous, saturating fluid with respect to a corotating coordinate system are given by

$$\mu \nabla^2 \mathbf{u}_f - \nabla p = \rho (\partial_t \mathbf{u}_f + \Omega \times (\Omega \times \mathbf{U}_f) + 2\Omega \times \mathbf{u}_f), \quad (S3)$$

where $\mathbf{u}_f = \partial_t \mathbf{U}_f$ is the acoustic fluid velocity associated with the displacement \mathbf{U}_f . Since the pore scale is much smaller than the acoustic scale, the fluid density ρ is taken to be constant here, and compressibility of the fluid is neglected. After obtaining an explicit permeability tensor, we will return to the description defined by (S1) and (S2), which takes into account compressibility.

Taking an intrinsic average of (S3) over a representative volume element (RVE) containing many pores, one concludes that a linear relationship exists between ∇p and the intrinsic average fluid velocity $\langle \mathbf{u}_f \rangle$:

$$\nabla p = -\mathbf{H}(\bar{\omega}, \Omega) \langle \mathbf{u}_f \rangle + \mathcal{O}(l/L), \quad (S4)$$

where l is the characteristic pore scale, L is the macroscopic scale, and $\mathbf{H} = \mu \mathbf{K}^{-1}$ [8]. Auriault notes a characteristic frequency $\omega_c = \mu/\rho_0 l^2$, and distinguishes between the low frequency regime $\bar{\omega} < \omega_c$, where viscous effects are dominant, and the high frequency regime $\bar{\omega} > \omega_c$, where inertial effects are dominant.

In the high frequency regime, one can neglect the viscous term in (S3). Straightforward averaging of the re-

sulting equation then leads to the lowest-order expression

$$-\varphi \nabla p = \rho_0 \left[-i\bar{\omega} \langle \mathbf{u}_f \rangle - \boldsymbol{\Omega} \times \left(\boldsymbol{\Omega} \times \frac{\langle \mathbf{u}_f \rangle}{i\bar{\omega}} \right) + 2\boldsymbol{\Omega} \times \langle \mathbf{u}_f \rangle \right], \quad (\text{S5})$$

implying that $\mathbf{H} = \frac{-i\bar{\omega}\rho_0}{\varphi} \mathbf{A}$, where \mathbf{A} has components

$$A_{ij} = \left(1 + \frac{\Omega^2}{\bar{\omega}^2} \right) \delta_{ij} - \frac{1}{\bar{\omega}^2} \Omega_i \Omega_j - \frac{2i}{\bar{\omega}} \epsilon_{ijn} \Omega_n. \quad (\text{S6})$$

The real part of \mathbf{H} relates to dissipation, whereas the imaginary part has inertial origins. One can see from (S6) that the high frequency regime has a primarily imaginary \mathbf{H} , with real contributions coming solely from the Coriolis term.

At this point, Auriault proceeds to determine $\mathbf{K}(\bar{\omega}, \boldsymbol{\Omega})$ for a particular idealized pore geometry composed of plane fissures, by solving the boundary value problem at the pore scale, and averaging the solution. Pore geometries one encounters in practice are often too complicated for the boundary value problem at the pore scale to be tractable, so we will instead observe from the linearity of (S3) that \mathbf{H} can be written in the form

$$\mathbf{H}(\bar{\omega}, \boldsymbol{\Omega}) = \mathbf{H}^0 - \frac{i\bar{\omega}\rho_0}{\varphi} \mathbf{A}(\bar{\omega}, \boldsymbol{\Omega}), \quad (\text{S7})$$

where \mathbf{H}^0 arises due to viscosity. For a macroscopically isotropic medium, neglecting the inertial terms leads to $\mathbf{H} = \mathbf{H}^0 = \frac{\mu}{K_0} \boldsymbol{\delta}$, with $\boldsymbol{\delta}$ denoting the unit tensor. This case represents the quasi-stationary, isotropic form of Darcy's filtration law, usually expressed as

$$\mathbf{v} = -\frac{K_0}{\mu} \nabla p, \quad (\text{S8})$$

with $\mathbf{v} = \langle \mathbf{u}_f \rangle$ being the filtration velocity. The quantity K_0 can be interpreted as the *static* permeability of the disk.

We can therefore obtain a macroscopic description of acoustics in the rotating porous disk by including both viscous and inertial terms in $\mathbf{H} \equiv \mu \mathbf{K}^{-1}$:

$$\mathbf{H}(\bar{\omega}, \boldsymbol{\Omega}) = \frac{\mu}{K_0} \boldsymbol{\delta} - \frac{i\bar{\omega}\rho_0}{\varphi} \mathbf{A}(\bar{\omega}, \boldsymbol{\Omega}), \quad (\text{S9})$$

with \mathbf{A} defined by (S6). The components of the resulting generalized Darcy law $\nabla p = -\mathbf{H}(\bar{\omega}, \boldsymbol{\Omega})\mathbf{v}$ can be expressed in cylindrical coordinates as

$$\partial_r p = \frac{i\bar{\omega}\rho_0}{\varphi} \left[\left(1 + \frac{\Omega^2}{\bar{\omega}^2} \right) v_r - 2i \frac{\Omega}{\bar{\omega}} v_\theta \right] - \frac{\mu}{K_0} v_r, \quad (\text{S10})$$

$$\frac{1}{r} \partial_\theta p = \frac{i\bar{\omega}\rho_0}{\varphi} \left[\left(1 + \frac{\Omega^2}{\bar{\omega}^2} \right) v_\theta + 2i \frac{\Omega}{\bar{\omega}} v_r \right] - \frac{\mu}{K_0} v_\theta, \quad (\text{S11})$$

$$\partial_z p = \left(\frac{i\bar{\omega}\rho_0}{\varphi} - \frac{\mu}{K_0} \right) v_z, \quad (\text{S12})$$

and the volume-balance equation (S1) can be written as

$$-\beta \left(\frac{\bar{\omega}}{c} \right)^2 p = \frac{i\bar{\omega}\rho_0}{\varphi} \left[\frac{1}{r} \partial_r (r v_r) + \frac{1}{r} \partial_\theta v_\theta + \partial_z v_z \right]. \quad (\text{S13})$$

The coupled equations (S10)-(S13) can be reduced to a

single acoustic equation expressed solely in terms of the pressure by inserting (S2) into (S1):

$$\beta \left(\frac{\bar{\omega}}{c} \right)^2 p = \frac{i\bar{\omega}\rho_0}{\mu\varphi} \nabla \cdot [\mathbf{K} \nabla p]. \quad (\text{S14})$$

The antisymmetric parts of \mathbf{K} cancel out in (S14) due to symmetry, leaving the diagonal components as the only contributors. Explicit expressions for the cylindrical components of \mathbf{K} can be found by inverting the matrix representation of (S9) in the (r, θ, z) basis.

Instead of working with the permeability directly, we will follow the description of the rigid-frame limit of Biot's theory, in which sound propagation in the porous medium is fully characterized by the compressibility $\beta(\bar{\omega})$ and the (tensor-valued) tortuosity $\boldsymbol{\alpha}(\bar{\omega}) = (i\varphi\mu/\bar{\omega}\rho_0)\mathbf{K}$. The pressure equation (S14) then becomes

$$-\beta \left(\frac{\bar{\omega}}{c} \right)^2 p = \nabla \cdot [\boldsymbol{\alpha}^{-1} \nabla p]. \quad (\text{S15})$$

The corresponding cancellation of off-diagonal elements for $\boldsymbol{\alpha}$ implies (S15) reduces to

$$-\beta \left(\frac{\bar{\omega}}{c} \right)^2 p = \alpha_{rr}^{-1} \frac{1}{r} \partial_r (r \partial_r p) + \alpha_{\theta\theta}^{-1} \partial_\theta^2 p + \alpha_{zz}^{-1} \partial_z^2 p. \quad (\text{S16})$$

Using the ansatz $p \sim J_m(k_{rr}) e^{-im\theta} e^{-ik_z z}$ in (S16) and noting that $\alpha_{rr}^{-1} = \alpha_{\theta\theta}^{-1}$ for isotropic media yields the dispersion relation

$$\beta \left(\frac{\bar{\omega}}{c} \right)^2 = \alpha_{rr}^{-1} k_r^2 + \alpha_{zz}^{-1} k_z^2. \quad (\text{S17})$$

To proceed further, we must invert the matrix formed by cylindrical components of \mathbf{H} . Fortunately, \mathbf{H} is block diagonal with respect to the axial (z) and transverse ($\{r, \theta\}$) coordinates. From the z -component (S12) of $\nabla p = -\mathbf{H}\mathbf{v}$ we immediately have $H_{zz}^{-1} = (H_{zz})^{-1} = \left(\frac{\mu}{K_0} - \frac{i\bar{\omega}\rho_0}{\varphi} \right)^{-1}$. The remaining transverse block of \mathbf{H} will be denoted by \mathbf{H}_\perp , such that

$$\mathbf{H}_\perp = \begin{pmatrix} \frac{\mu}{K_0} - \frac{i\bar{\omega}\rho_0}{\varphi} \left(1 + \frac{\Omega^2}{\bar{\omega}^2} \right) & -\frac{2\Omega\rho_0}{\varphi} \\ \frac{2\Omega\rho_0}{\varphi} & \frac{\mu}{K_0} - \frac{i\bar{\omega}\rho_0}{\varphi} \left(1 + \frac{\Omega^2}{\bar{\omega}^2} \right) \end{pmatrix}. \quad (\text{S18})$$

The inverse is given by a similar expression, but with the signs of the off-diagonal elements swapped and an overall factor of $(\det \mathbf{H}_\perp)^{-1} = (H_{rr}^2 + H_{r\theta}^2)^{-1}$ in front.

Defining $\bar{\omega}_c = \mu\varphi/\rho_0 K_0$ and $\bar{\omega}_\Omega = \bar{\omega}(1 + \Omega^2/\bar{\omega}^2)$, the components of $\boldsymbol{\alpha}^{-1}$ relevant to completing specification of the dispersion relation (S17) can be written

$$\alpha_{zz}^{-1} = \frac{-i\bar{\omega}}{\bar{\omega}_c - i\bar{\omega}} \quad (\text{S19})$$

and

$$\alpha_{rr}^{-1} = \frac{-i\bar{\omega} (\bar{\omega}_c - i\bar{\omega}_\Omega)}{[(\bar{\omega}_c - i\bar{\omega}_\Omega)^2 + 4\Omega^2]}. \quad (\text{S20})$$

Interface Conditions and the Surface Impedance

The surface of our porous disk is at $z = 0$, with the pure-fluid region (hereafter be referred to as “region I”) occupying the positive z half-space within the tube of radius R . Conservation of fluid mass implies continuity of the normal fluid displacement at the $z = 0$ fluid-disk interface, since we are neglecting small variations in the density. For harmonic acoustic modes, we can equivalently enforce continuity of the normal fluid velocity. In the porous disk region (hereafter referred to as “region II”), we denote the co-rotating axial wavenumber by \bar{k}_z and the co-rotating radial wavenumber by \bar{k}_r . We will also suppose the disk is thick enough that the transmitted wave attenuates fast enough to ignore reflections from the rigid backing. Specifically, the pressure in region II will be expressed as

$$p = \alpha_- J_{\bar{m}}(\bar{k}_r r) e^{i\bar{m}\bar{\theta}} e^{-i\bar{k}_z z} e^{-i\bar{\omega}t}, \quad (\text{S21})$$

where $\bar{\theta} = \theta - \Omega t$, with θ being the azimuthal angle defined with respect to the nonrotating (laboratory) coordinate system. In region I, the acoustic fluid velocity field is $\mathbf{u} = \nabla\Phi$, and the acoustic pressure is $p = i\omega\rho_0\Phi$, with the potential Φ given by

$$\Phi = J_m(k_r r) e^{im\theta} (\alpha^- e^{-ik_z z} + \alpha^+ e^{ik_z z}) e^{-i\omega t}. \quad (\text{S22})$$

Since only a fraction φ of the disk volume is occupied by the saturating fluid, one can distinguish between the filtration velocity \mathbf{v} and the intrinsic fluid velocity \mathbf{V} , obtained by averaging only over pores themselves. The two types of averages are connected by the Dupuit-Forchheimer relationship, $\mathbf{v} = \varphi\mathbf{V}$, which expresses quantitatively the difference between averaging the pore-scale fluid velocity over the whole RVE and averaging just over the pores [7]. Therefore, the correct normal velocity continuity expression is

$$\mathbf{u} \cdot \hat{\mathbf{z}}|_{z=0^+} = \mathbf{v} \cdot \hat{\mathbf{z}}|_{z=0^-}. \quad (\text{S23})$$

Continuity of the acoustic fluid pressure will also be enforced at the interface, such that

$$p|_{z=0^+} = p|_{z=0^-}. \quad (\text{S24})$$

Pressure continuity then implies $\bar{k}_r = k_r$, $\bar{m} = m$, $\bar{\omega} = \omega - m\Omega$, and

$$\alpha_- = i\omega\rho_0 (\alpha^+ + \alpha^-), \quad (\text{S25})$$

and using (S12), continuity of normal velocity implies

$$\frac{\bar{k}_z\alpha_-}{\left(\frac{\mu}{K_0} - \frac{i\bar{\omega}\rho_0}{\varphi}\right)} = k_z (\alpha^+ - \alpha^-). \quad (\text{S26})$$

Combining (S25) and (S26), we find

$$k_z (\alpha^+ - \alpha^-) = -\hat{k}_z (\alpha^+ + \alpha^-), \quad (\text{S27})$$

with the definition

$$\hat{k}_z = \frac{i\omega\rho_0\bar{k}_z K_0\varphi}{i\bar{\omega}\rho_0 K_0 - \mu\varphi} = \frac{\omega\varphi\bar{k}_z}{\bar{\omega} + i\bar{\omega}_c}. \quad (\text{S28})$$

It follows that the reflection amplitude α^+/α^- is given by

$$\frac{\alpha^+}{\alpha^-} = \frac{k_z - \hat{k}_z}{k_z + \hat{k}_z}. \quad (\text{S29})$$

The surface impedance is defined as $Z = \frac{-p}{\mathbf{u} \cdot \hat{\mathbf{n}}}$, with $\hat{\mathbf{n}}$ being the unit surface normal. Note that this interpretation of surface impedance allows a coupling between the monochromatic modes in the pipe to *both* the irrotational and vortical modes in the disk, which did not occur in previous work [5]. In our case $\hat{\mathbf{n}} = \hat{\mathbf{z}}$, which leads to the expressions

$$Z = \frac{\rho_0\omega}{\bar{k}_z} = \frac{\rho_0\bar{\omega}}{\varphi\bar{k}_z} \left(1 + \frac{i\bar{\omega}_c}{\bar{\omega}}\right). \quad (\text{S30})$$

The impedance (S30) can also be used to express the reflection amplitude as

$$\frac{\alpha^+}{\alpha^-} = \frac{Z - \frac{\rho_0\omega}{\bar{k}_z}}{Z + \frac{\rho_0\omega}{\bar{k}_z}}. \quad (\text{S31})$$

Using the dispersion relation (S17), we can write the factor $1/\bar{k}_z$ as

$$\frac{1}{\bar{k}_z} = \frac{\sqrt{\alpha_{zz}^{-1}}}{\sqrt{\beta\left(\frac{\bar{\omega}}{c}\right)^2 - \alpha_{rr}^{-1}\bar{k}_r^2}}, \quad (\text{S32})$$

and to be completely explicit, we can write the impedance (S30) as

$$Z = \frac{\rho_0\bar{\omega}\sqrt{\alpha_{zz}^{-1}}}{\varphi\sqrt{\beta\left(\frac{\bar{\omega}}{c}\right)^2 - \alpha_{rr}^{-1}\bar{k}_r^2}} \left(1 + \frac{i\bar{\omega}_c}{\bar{\omega}}\right), \quad (\text{S33})$$

with α_{zz}^{-1} and α_{rr}^{-1} given by (S19) and (S20), respectively.

The amplification factor $A_{\omega m} = |\alpha^+/\alpha^-|^2 - 1$ can now be determined, using (S31) and (S33). First, we will rewrite (S31) as

$$\frac{\alpha^+}{\alpha^-} = \frac{1 - \chi}{1 + \chi}, \quad (\text{S34})$$

with the definition $\chi = \rho_0\omega/k_z Z$. Then we can write the amplification as

$$A_{\omega m} = \frac{-4\text{Re}[\chi]}{|1 + \chi|^2} = \frac{-4\text{Re}[\chi^{-1}]}{|\chi(1 + \chi)|^2}, \quad (\text{S35})$$

from which we can deduce that positive amplification occurs when the real part of $k_z Z$ is negative. The quantity χ can be written

$$\chi = \frac{\varphi\omega\bar{k}_z}{(\bar{\omega} + i\bar{\omega}_c)k_z} = \frac{\varphi\omega(\bar{\omega} - i\bar{\omega}_c)\bar{k}_z}{(\bar{\omega}^2 + \bar{\omega}_c^2)k_z}, \quad (\text{S36})$$

which allows us to express the amplification factor as

$$A_{\omega m} = \frac{-4(\bar{\omega}^2 + \bar{\omega}_c^2)^2 |k_z|^4 (\bar{\omega}\text{Re}[k_z^*\bar{k}_z] + \bar{\omega}_c\text{Im}[k_z^*\bar{k}_z])}{\omega^3\varphi^3|\bar{k}_z|^4 |(\bar{\omega} + i\bar{\omega}_c)k_z + \omega\varphi\bar{k}_z|^2}. \quad (\text{S37})$$

We therefore see from (S37) that if k_z is real, positive amplification occurs whenever $\bar{\omega}\text{Re}[\bar{k}_z] + \bar{\omega}_c\text{Im}[\bar{k}_z] < 0$.

If k_z is purely imaginary, however, positive amplification occurs whenever $\text{Im}[k_z](\bar{\omega}\text{Im}[\bar{k}_z] - \bar{\omega}_c\text{Re}[\bar{k}_z]) < 0$.

Radial Constraint Transformation

Care must be taken in region II when applying the radial impermeability constraint at $r = R$, since the velocity vector is defined with respect to the rotating frame. In region I, the condition $u_r|_{r=R} = 0$ implies $J'_m(k_r R) = 0$. In region II, due to rotation, we have

$$u_r|_{r=R} = \left[-H_{rr}^{-1} \partial_r p - H_{r\bar{\theta}}^{-1} \frac{1}{r} \partial_{\bar{\theta}} p \right]_{r=R}, \quad (\text{S38})$$

the vanishing of which would require

$$-H_{rr}^{-1} \bar{k}_r J'_{\bar{m}}(\bar{k}_r R) + H_{r\bar{\theta}}^{-1} \frac{i\bar{m}}{R} J_{\bar{m}}(\bar{k}_r R) = 0. \quad (\text{S39})$$

However, continuity of acoustic pressure demands $\bar{k}_r = k_r$ and $\bar{m} = m$, which means $J'_{\bar{m}}(\bar{k}_r R) = 0$. It would then not be possible to satisfy the radial constraint (S39), since it has been reduced to $J_{\bar{m}}(\bar{k}_r R) = 0$, which will generally not be true.

The preceding issue is easily resolved by transforming the fluid velocity back into the laboratory frame. Denoting the rotating cylindrical basis vectors by $\{\bar{\mathbf{e}}_j\}$ and the cylindrical laboratory basis vectors by $\{\mathbf{e}_j\}$, we first note that if the fluid velocity is $\mathbf{v} = \partial_t \mathbf{U}$ with respect to the rotating coordinate system, then from the perspective of a stationary observer the fluid velocity is

$$(\partial_t \mathbf{U})_I = \partial_t (\bar{U}_j \bar{\mathbf{e}}_j) = \dot{\bar{U}}_j \bar{\mathbf{e}}_j + \bar{U}_j \dot{\bar{\mathbf{e}}}_j, \quad (\text{S40})$$

where Einstein summation is assumed and an overdot indicates a time derivative. The rotating frame has angular velocity $\boldsymbol{\Omega}$, and the quantity $\dot{\bar{U}}_j \bar{\mathbf{e}}_j$ is simply the velocity with respect to the rotating frame, so the stationary-frame velocity (S40) takes the more intuitive form

$$(\partial_t \mathbf{U})_I = \mathbf{v} + \boldsymbol{\Omega} \times \mathbf{U}. \quad (\text{S41})$$

If the velocity is harmonic in time with frequency $\bar{\omega}$, then the displacement \mathbf{U} can be written $\mathbf{U} = \mathbf{v}/(-i\bar{\omega})$, and in cylindrical coordinates the transformation (S41) becomes

$$\begin{aligned} (\partial_t \mathbf{U})_I &= \mathbf{v} - \frac{\Omega}{i\bar{\omega}} (\bar{v}_r \bar{\mathbf{e}}_\theta - \bar{v}_\theta \bar{\mathbf{e}}_r) \\ &= \left(\bar{v}_r + \frac{\Omega}{i\bar{\omega}} \bar{v}_\theta \right) \bar{\mathbf{e}}_r + \left(\bar{v}_\theta - \frac{\Omega}{i\bar{\omega}} \bar{v}_r \right) \bar{\mathbf{e}}_\theta + \bar{v}_z \bar{\mathbf{e}}_z. \end{aligned} \quad (\text{S42})$$

Finally, one can switch to the laboratory basis if desired, using the relations $\bar{\mathbf{e}}_r = \mathbf{e}_r|_{\theta=\bar{\theta}+\Omega t}$, $\bar{\mathbf{e}}_\theta = \mathbf{e}_\theta|_{\theta=\bar{\theta}+\Omega t}$, $\bar{\mathbf{e}}_z = \mathbf{e}_z$.

Asymptotic Behaviour

To gain intuition about the physics contained in the expressions for the impedance (S33) and the reflection amplitude (S29), we consider their behaviour in the low and

high frequency regimes defined by $\bar{\omega} \ll \bar{\omega}_c$ and $\bar{\omega} \gg \bar{\omega}_c$, respectively. Viscous effects dominate the low frequency regime, so in this limit we imagine $\bar{\omega}_c \rightarrow \infty$, which also coincides with the impermeable ($K_0 \rightarrow 0$) limit. In this case, we have

$$\alpha_{zz}^{-1} \sim -i \frac{\bar{\omega}}{\bar{\omega}_c} \left(1 + \frac{i\bar{\omega}}{\bar{\omega}_c} \right) \quad (\text{S43})$$

and

$$\alpha_{rr}^{-1} \sim -i \frac{\bar{\omega}}{\bar{\omega}_c} \left(1 + \frac{i\bar{\omega}_\Omega}{\bar{\omega}_c} \right), \quad (\text{S44})$$

which implies that

$$\sqrt{\alpha_{zz}^{-1}} \sim \sqrt{-i \frac{\bar{\omega}}{\bar{\omega}_c}} \left(1 + \frac{i\bar{\omega}}{2\bar{\omega}_c} \right) \quad (\text{S45})$$

and

$$\sqrt{\beta \left(\frac{\bar{\omega}}{c} \right)^2 - \alpha_{rr}^{-1} k_r^2} \sim \sqrt{\beta \left(\frac{\bar{\omega}}{c} \right)^2 + \frac{i\bar{\omega}}{\bar{\omega}_c} k_r^2}. \quad (\text{S46})$$

We then have the limiting impedance behaviour

$$Z \sim \frac{\rho_0 i\bar{\omega}_c}{\varphi \sqrt{i\beta \frac{\bar{\omega}\bar{\omega}_c}{c^2} - k_r^2}}. \quad (\text{S47})$$

From here, there are two possible limits, depending on the size of k_r^2 compared to $\bar{\omega}\bar{\omega}_c/c^2$. If $k_r^2 \gg \bar{\omega}\bar{\omega}_c/c^2$, then

$$Z \rightarrow \frac{\rho_0 \bar{\omega}_c}{\varphi k_r}. \quad (\text{S48})$$

This leads to a reflection amplitude limit

$$\frac{\alpha^+}{\alpha_-} \rightarrow \frac{\left(\frac{\bar{\omega}_c}{\varphi k_r} - \frac{\omega}{k_z} \right)}{\left(\frac{\bar{\omega}_c}{\varphi k_r} + \frac{\omega}{k_z} \right)}, \quad (\text{S49})$$

which approaches unity for small laboratory-frame frequencies ($\omega \rightarrow 0$). Conversely, if $k_r^2 \ll \bar{\omega}\bar{\omega}_c/c^2$, then

$$Z \rightarrow \frac{\rho_0 c}{\varphi} \sqrt{\frac{i\bar{\omega}_c}{\beta\bar{\omega}}}, \quad (\text{S50})$$

which corresponds to a reflection amplitude

$$\frac{\alpha^+}{\alpha_-} \rightarrow \frac{\left(\frac{c}{\varphi} \sqrt{\frac{i\bar{\omega}_c}{\beta\bar{\omega}}} - \frac{\omega}{k_z} \right)}{\left(\frac{c}{\varphi} \sqrt{\frac{i\bar{\omega}_c}{\beta\bar{\omega}}} + \frac{\omega}{k_z} \right)}. \quad (\text{S51})$$

As $\omega \rightarrow 0$, the reflection (S51) approaches unity as well.

The high frequency limit is equivalent to $\bar{\omega}_c \rightarrow 0$, which also coincides with the highly permeable limit $K_0 \rightarrow \infty$. One then finds $\alpha_{zz}^{-1} \rightarrow 1$ and

$$\alpha_{rr}^{-1} \rightarrow \frac{\left(1 + \frac{\Omega^2}{\bar{\omega}^2} \right)}{\left(1 - \frac{\Omega^2}{\bar{\omega}^2} \right)^2}. \quad (\text{S52})$$

Making the definition

$$\hat{k}_r^2 = k_r^2 \frac{\left(1 + \frac{\Omega^2}{\bar{\omega}^2} \right)}{\left(1 - \frac{\Omega^2}{\bar{\omega}^2} \right)^2}, \quad (\text{S53})$$

we further have $\hat{k}_z \rightarrow \varphi \bar{k}_z$ and $\bar{k}_z \rightarrow \sqrt{\beta(\bar{\omega}/c)^2 - \hat{k}_r^2}$. The impedance is then given by the limiting expression

$$Z \rightarrow \frac{\rho_0 \bar{\omega}}{\varphi \bar{k}_z} = \frac{\rho_0 c}{\varphi} \frac{\bar{\omega}}{\sqrt{\beta \bar{\omega}^2 - \hat{k}_r^2 c^2}}. \quad (\text{S54})$$

The corresponding reflection amplitude in this limit is

$$\begin{aligned} \frac{\alpha^+}{\alpha^-} &\rightarrow \frac{k_z - \varphi \bar{k}_z}{k_z + \varphi \bar{k}_z} \\ &= \frac{\sqrt{\left(\frac{\omega}{c}\right)^2 - k_r^2} - \varphi \sqrt{\beta \left(\frac{\bar{\omega}}{c}\right)^2 - \hat{k}_r^2}}{\sqrt{\left(\frac{\omega}{c}\right)^2 - k_r^2} + \varphi \sqrt{\beta \left(\frac{\bar{\omega}}{c}\right)^2 - \hat{k}_r^2}}. \end{aligned} \quad (\text{S55})$$

When $\bar{\omega} \rightarrow \infty$, $\hat{k}_r^2 \rightarrow k_r^2$, and the reflection amplitude (S55) vanishes, as expected. For finite $\bar{\omega}$, the amplification (S37) behaves as

$$A_{\omega m} \rightarrow \frac{-4\bar{\omega}^5 |k_z|^4 \text{Re}[k_z^* \bar{k}_z]}{\omega^3 \varphi^3 |\bar{k}_z|^4 |\bar{\omega} k_z + \omega \varphi \bar{k}_z|^2}. \quad (\text{S56})$$